Structure and Dynamics of S_2 and S_1 Diphenylacetylene in Solution Studied by Picosecond Time-Resolved CARS Spectroscopy

Taka-aki Ishibashi and Hiro-o Hamaguchi*

Department of Chemistry, School of Science, The University of Tokyo, 7-3-1 Hongo 113, Japan

Received: August 28, 1997; In Final Form: January 15, 1998

Picosecond time-resolved CARS spectra of diphenylacetylene and its ^{13}C-substituted analogue in cyclohexane are reported for the 2330−590 cm^{-1} wavenumber shift. The transient CARS bands of the S_2 and S_1 states are observed in addition to those of the cation radical, the anion radical, and the T_1 state. It is found that the central CC stretch frequency of the S_1 state is smaller than 1600 cm^{-1}, indicating a marked decrease of the CC bond order in this state. The width of the central CC stretch band of the S_2 state is found to be ∼40 cm^{-1} (hwhm). These spectral features are discussed in connection with the structure and dynamics in the two singlet excited states.

1. Introduction

Diphenylacetylene (DPA) is one of the most fundamental aromatic molecules that have a CC triple bond. DPA has a strong electronic absorption band in the 300−250 nm region. This band has been assigned to the 1^1B_{1u} state (polarized parallel to the long axis of the molecule) by dichroic absorption measurements in stretched poly(vinyl alcohol) sheets.[1] From the mirror image relation of the fluorescence spectra to the absorption, the 1^1B_{1u} state is considered to be responsible for the fluorescence.

Okuyama et al. reported the fluorescence excitation, dispersed fluorescence, and multiphoton ionization spectra of DPA in a supersonic jet.[2] They found that three excited singlet states exist within a range of a few hundred wavenumbers. The highest one of the three states was assigned to the 1^1B_{1u} state, which is fully one-photon-allowed from the ground state. The other two low-lying states were assigned to the weakly one-photon-allowed 1^1B_{2u} state and the two-photon-allowed 2^1A_g state,[2] respectively, on the basis of the semiempirical CI calculation including only π-orbitals perpendicular to the molecular plane.[1] No fluorescence and one-photon resonant ionization signals were detected when the excitation energy was higher than ∼1000 cm^{-1} from the 1^1B_{1u} band origin. From this observation, Okuyama et al. concluded that an extremely rapid relaxation process exists in the region above ∼1000 cm^{-1}. This work was followed by several extensive studies of the singlet excited states of DPA in the condensed phase.[3−7] Gutmann et al. observed the dispersed fluorescence and one-photon and two-photon resonant fluorescence excitation spectra of DPA isolated in low-temperature matrixes and analyzed them on the basis of semiempirical CI calculations.[3] They suggested that (1) the S_1 state of DPA in matrixes is the 1^1B_{1u} state, which was thought to be the S_3 state in a supersonic jet, (2) the two-photon resonant fluorescence of DPA in matrixes is from the b_{2u} vibrational levels of the 1^1B_{1u} manifold that are vibronically coupled with the 1^1B_{3g} state, and (3) the two-photon resonant ionization signal of DPA in a supersonic jet can be due to the 1^1A_u manifold. A few months after the publication of this work, Hirata et al. reported the results of their picosecond time-resolved absorption and fluorescence lifetime measurements of DPA in solutions[4] that contradicted the conclusion of the matrix study. They observed two transient absorption bands with different lifetimes that were assigned to the S_2 and S_1 states. The S_2 state has a lifetime of ∼9 ps in cyclohexane at room temperature and is converted to the S_1 state by the internal conversion process that has an activation energy of ∼1000 cm^{-1}. The S_2 state, and not the S_1 state, was considered to be the optically allowed 1^1B_{1u} state, because the decay constant of the S_2 absorption agreed with that of the fluorescence.

To explain this contradiction of the assignments of the excited singlet states, Ferrante et al. proposed a model based on semiempirical CI potentials of the excited singlet states.[7] In their model, the S_2 and S_1 state were regarded as "isomers" having different central CC bond lengths. The observed activation energy for internal conversion was ascribed to the crossing of the 1^1B_{1u} and 1^1A_u potentials along the CC coordinate. The 1^1B_{1u} state is the S_2 state and the 1^1A_u state is the S_1 state energetically, though the former becomes the lowest excited singlet state at the CC bond length of the ground state. According to Ferrante et al., the apparent contradiction will be solved if the "isomerization" is prohibited in low-temperature matrixes or if the 1^1B_{1u} state is stabilized significantly by the matrix effect. Although their model gives a likely explanation for the experimental contradictions in matrixes and solution, it is yet to be experimentally verified. Vibrational spectra of the S_2 and S_1 states are expected to afford direct structural information. Hiura and Takahashi observed spontaneous Raman spectra of the cation radical, the anion radical, and the lowest excited triplet (T_1) state of DPA in solution, but they were not able to observe the spectra of the excited singlet states because of the hindrance by strong fluorescence.[8]

In a previous letter,[9] we reported the central CC stretch frequencies of the S_2 and S_1 DPA in cyclohexane determined by picosecond time-resolved CARS spectroscopy. The very low CC stretch frequency (<1600 cm^{-1}) in the S_1 state was consistent with the theoretical prediction.[7] In this paper we report the full region (2330−590 cm^{-1}) of the CARS spectra of S_2 and S_1 DPA in cyclohexane and discuss the structure of the excited singlet states in connection with the $S_2 \rightarrow S_1$ internal conversion process.

S1089-5639(97)02809-0 CCC: $15.00
Published on Web 03/07/1998

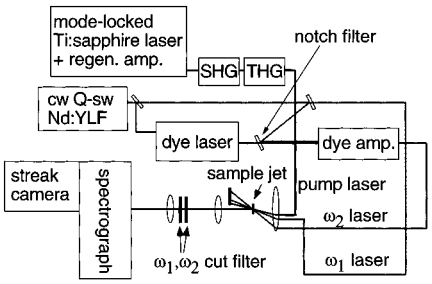

Figure 1. Block diagram of picosecond time-resolved 2D CARS setup.

2. Experimental Section

Measuring Method. We used the picosecond 2D multiplex CARS technique[10] to obtain time-resolved CARS spectra. In this technique, the transient species generated by a sub-picosecond laser pulse are monitored by nanosecond CARS probing lasers ($\omega_1 > \omega_2$; ω_1 is narrow-band and ω_2 broad-band). The CARS signals are spectrally resolved by a polychromator and temporally resolved by a streak camera.

The block diagram of the 2D CARS setup is shown in Figure 1. The third harmonic of a regeneratively amplified mode-locked Ti:sapphire laser (Clark-MXR RA1, ~270 nm, <1 ps, 1 kHz) was used as the pump laser to photoexcite the sample. The CARS probing laser system was based on a diode-pumped CW Q-switched Nd:YLF laser (Spectra Physics TFR, 523.5 nm, ~5 ns, 1 kHz). The second harmonic of the Nd:YLF laser was split into three parts. The first part (~20 mW) was used as the ω_1 laser of the CARS probing. The second part (~5 mW) pumped the broad-band dye laser (Spectra Physics 375B). The dye laser cavity was modified to obtain broad-band output; the wavelength tuning element was removed, and the cavity length of the oscillator was reduced. The output (~0.5 mW, ~5 ns) of the dye laser was amplified by a homemade dye amplifier pumped by the third part of the second harmonic of the Nd:YLF laser (~50 mW). A perfect collinear pumping geometry was realized by using a notch filter (Solar) for 532 nm on which the dye laser output and the pumping laser were superimposed. The output of the dye amplifier was used as the ω_2 laser of the CARS probing.

The two CARS probe laser beams and the pump laser beam were focused on a thin jet flow of sample solution ejected from a dye laser nozzle. Typical power of the ω_1, ω_2, and pump laser was ~10, ~3, and ~1 mW respectively. The nanosecond broad-band CARS signal was separated from the pump and probe laser beams by a spatial filter (an iris) and optical filters. A holographic notch filter for 523.5 nm (Kaiser Optical Systems) and a band-pass filter for 510−420 nm (Vacuum Optics Corporation of Japan) were used as the optical filters. The signal was then dispersed by a polychromator (Chromex 500) and time-resolved by a streak camera (Hamamatsu Photonics modified C2909) with ~20 ps time resolution. The time and spectral profiles of the signal were recorded simultaneously on a CCD detector as a two-dimensional image.

Samples. Diphenylacetylene, $C_6H_5C{\equiv}CC_6H_5$ (normal-DPA), was obtained from Aldrich Chemical Co. and purified by recrystallization from ethanol before use. The ^{13}C-substituted analogue of DPA, $C_6H_5\ ^{13}C{\equiv}CC_6H_5$ (^{13}C-DPA), was prepared by the coupling of copper(I) phenylacetylide-*2*-^{13}*C* with iodobenzene. The copper(I) phenylacetylide-*2*-^{13}*C* was synthesized from phenylacetylene-*2*-^{13}*C* (ICON Services Inc.).[11,12] The synthesized ^{13}C-DPA was purified by silica gel column chromatography. Liquid chromatography grade cyclohexane was used as the solvent. All measurements were performed using 5 mmol/L cyclohexane solution of DPA.

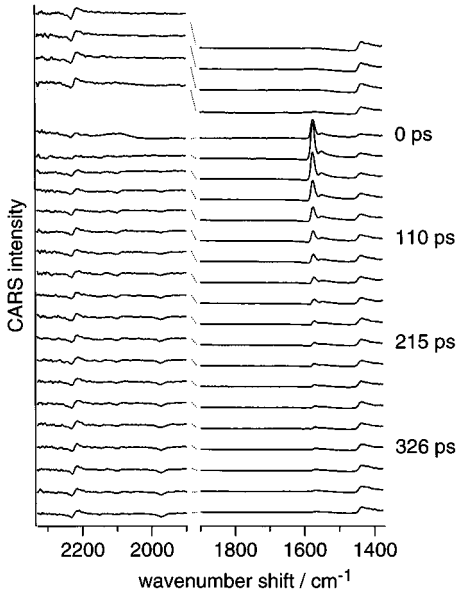

Figure 2. Picosecond time-resolved CARS spectra of normal-DPA in cyclohexane (5 mM). The time interval between two adjacent spectra: ~21 ps.

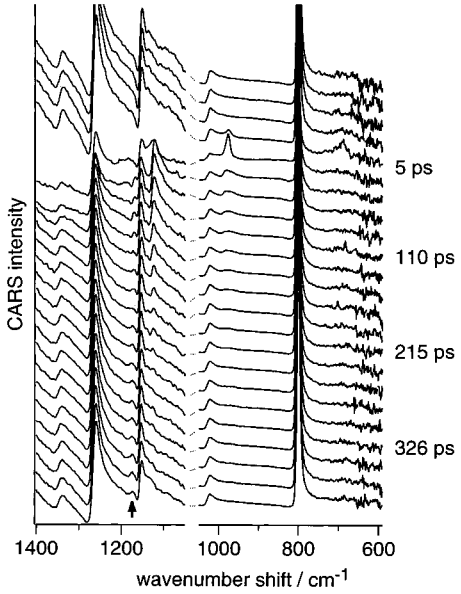

Figure 3. Picosecond time-resolved CARS spectra of normal-DPA in cyclohexane (5 mM). The time interval between two adjacent spectra: ~21 ps.

3. Results and Discussion

Time-Resolved Spectra and Assignments of Transient Species. Time-resolved CARS spectra of DPA photoexcited at 270 nm are shown in Figures 2 and 3. In these spectra, the spectral distribution of the ω_2 laser and the temporal profile of the ω_1 and ω_2 lasers are already corrected. The contribution from fluorescence was subtracted before the correction.[13] The nonresonant CARS signals of cyclohexane, carbon tetrachloride, and water were used for the correction in the 2330−1900, 1900−1150, and 1150−590 cm^{-1} regions, respectively. The CARS signal from solvent decreases for a few picoseconds after the photoexcitation and then increases gradually. This is due to the transient absorption and also to the scattering by the

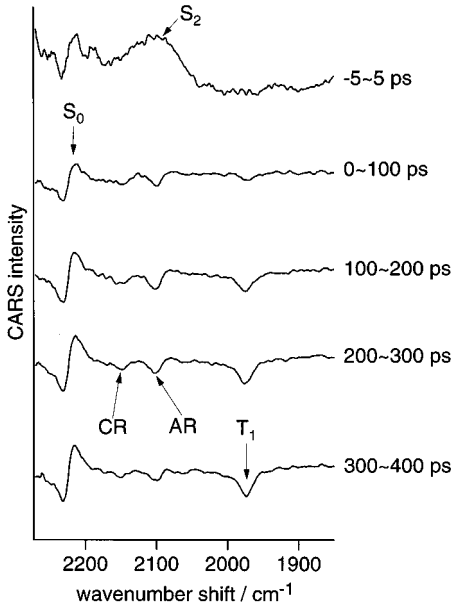

Figure 4. Time-resolved CARS spectra of the cation radical (CR), the anion radical (AR), and the T_1 state of normal-DPA in cyclohexane (5 mM).

thermal turbulence of the sample jet flow induced by the photoexcitation.

Two kinds of transient species with different lifetimes are found in Figures 2 and 3. The transient CARS bands of the shorter-lived species are observed at ∼2100 (very broad band), ∼1190, ∼1130, ∼980, and ∼690 cm^{-1} in the time-resolved spectra. The lifetime of the shorter-lived species is estimated to be less than ∼20 ps (the time resolution of our experiment setup), since the bands of this species are observed only just after the photoexcitation. The transient CARS bands of the longer-lived species are observed at ∼1570, ∼1120, and ∼970 cm^{-1}. The lifetime of this longer-lived species is estimated to be ∼200 ps as a result of the spectral simulations described in the next subsection. Because the estimated lifetimes of the shorter-lived and longer-lived species agree with the known lifetimes[4] of the S_2 (∼9 ps) and S_1 (∼200 ps) states, respectively, the shorter-lived species is identified as the S_2 state and the longer-lived species as the S_1 state. Note that resonance enhancements are expected for both of the S_2 and S_1 CARS signals either by the ω_1 resonance (523.5 nm) or by the CARS signal resonance (508−467 nm), because the $S_n \leftarrow S_2$ and $S_n \leftarrow S_1$ absorption maxima are located at 500 and 435 nm, respectively.[4]

In addition to the S_0 band at 2223 cm^{-1}, three transient CARS bands that cannot be assigned to the excited singlet states are observed in the 2200−1950 cm^{-1} region. To show these bands more clearly, the time-resolved CARS spectra averaged over each 100 ps are shown in Figure 4. These three bands are weak in intensity and appear as dips in the CARS spectra. All these bands show large downshifts (20−50 cm^{-1}) upon the ^{13}C-substitution. Candidates of the transient species to which these bands can be assigned are the cation radical, the anion radical, and the T_1 state of DPA. In fact, the dip positions coincide with the reported Raman frequencies[8] of the C≡C stretch vibrations of these transient species. Therefore, we assign these three bands to the anion radical (2091 cm^{-1}), the cation radical (2142 cm^{-1}), and the T_1 state (1974 cm^{-1}) of DPA, respectively. The intensity of the T_1 CARS band seems to increase with the time constant of the S_1 decay and shows no decrease in the time region 400 ps after the photoexcitation (Figure 4). This observation is consistent with the result of the time-resolved absorption study[4] in that the T_1 state is generated from the S_1 state through intersystem crossing. The kinetics of the cation radical and the anion radical are similar to each other, but different from that of the T_1 state. The band intensities (dip depth) of these radicals reach their maxima by the time 200 ps after the photoexcitation and then decrease gradually. It is interesting that the radical species are photogenerated in a nonpolar solvent such as cyclohexane. For further elucidation of the radical formation mechanism, it is necessary to examine the concentration dependence, the laser power dependence, and so on. Checking of the solvent purity is also necessary. These studies are left for future investigations.

In the 1170 cm^{-1} region, there is one band (marked by an arrow in Figure 3) that appears just after the photoexcitation and does not decrease in intensity even after 380 ps. This band shows a gradual shift during the period of 0−380 ps. It is possible that both the S_1 and T_1 states have CARS bands in the same 1170 cm^{-1} region. A Raman band of the T_1 state is reported in this wavenumber region.[8]

Spectral Simulation. In CARS spectroscopy, spectral simulations are necessary in order to determine the band parameters (vibrational frequency, bandwidth, and so on) from the observed CARS spectrum, because CARS band shapes are generally affected by the interference from the nonresonant term of the solvent, the electronic terms of the transients species, and the Raman terms of other vibrational bands. The CARS intensity is given by the square modulus of the CARS susceptibility. Here, we assume the following form of the CARS susceptibility (χ_{CARS}):

$$\chi_{CARS} = \chi_{solvent} + \chi_{S_0} + \sum_{TR} \chi_{TR}$$

where $\chi_{solvent}$, χ_{S_0}, and χ_{TR} are the susceptibilities of the solvent, S_0 DPA, and the photogenerated transient species of DPA. Lorentz functions are used as Raman resonance terms in each susceptibility. Precise forms of terms in χ_{CARS} are shown in Table 1. A second-order polynomial is used as an additional fitting function in order to correct the spectral distortion of the streak image.[14]

The simulation was carried out in the following manner. First, we determined the parameters of the solvent by simulating the CARS spectra of the solvent. Second, we determined the parameters of the S_0 DPA by simulating the CARS spectra of the solution without the photoexcitation. In the third step, we determined the parameters of the S_1 DPA by simulating the CARS spectra 40−60 ps after the photoexcitation. We can safely neglect the contribution to the spectra of this time region from the S_2 state DPA. In the last step, the parameters of the S_2 DPA were determined by simulating the CARS spectra −5 to 5 ps after the photoexcitation. If there was a sign of the existence of the S_1 DPA on the spectra of this time region, we took into account the contribution from S_1 DPA. Otherwise we neglected it. In the case of the simulation of the 2300−1900 cm^{-1} region, we also neglected the electronic term of the S_2 DPA susceptibility, because this term was hardly determinable due to the absence of the vibrational band of the solvent in this spectral region. The results of the spectral simulations are shown in Figure 5, for the spectra 40−60 ps after the photoexcitation, and in Figure 6 for the spectra −5 to 5 ps after the photoexcitation. The agreement between the observed and

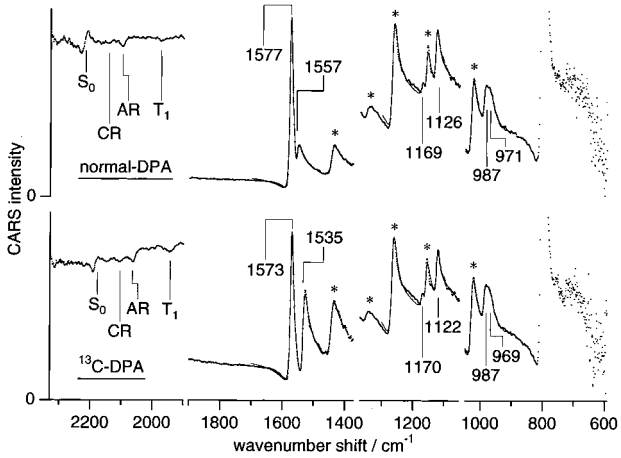

Figure 5. Observed and simulated CARS spectra of the S_1 DPA. Dots show observed data obtained 40−60 ps after the photoexcitation, solid lines simulated spectra. *: cyclohexane.

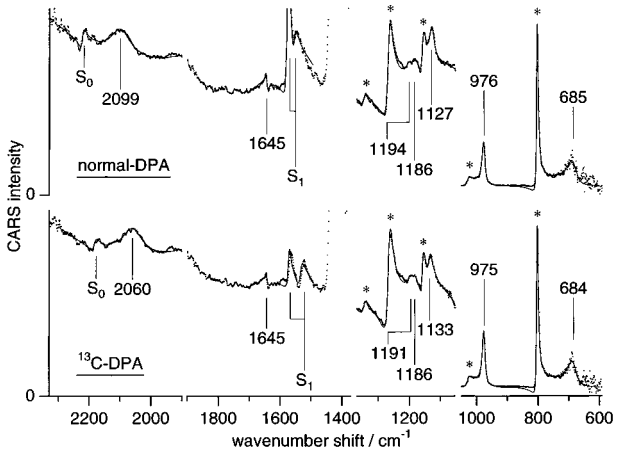

Figure 6. Observed and simulated CARS spectra of the S_2 DPA. Dots show observed data obtained −5 to 5 ps after the photoexcitation, solid lines simulated spectra. *: cyclohexane.

TABLE 1: CARS Susceptibility

$$\chi_{\mathrm{CARS}} = \chi_{\mathrm{solvent}} + \chi_{\mathrm{S_0}} + \sum_{\mathrm{TR}} \chi_{\mathrm{TR}}$$

Susceptibility of Solvent

$$\chi_{\mathrm{solvent}} = \chi^{\mathrm{NR}}_{\mathrm{solvent}} + \chi^{\mathrm{R}}_{\mathrm{solvent}}$$

(nonresonant term) $\chi^{\mathrm{NR}}_{\mathrm{solvent}}$: real constant

$$\text{(Raman term) } \chi^{\mathrm{R}}_{\mathrm{solvent}} = \sum_i \frac{A_i}{\Omega_i - (\omega_1 - \omega_2) + \mathrm{i}\Gamma_i}$$

Susceptibility of S_0 DPA

$$\chi_{\mathrm{S_0}} = \chi^{\mathrm{NR}}_{\mathrm{S_0}} + \chi^{\mathrm{R}}_{\mathrm{S_0}}$$

(nonresonant term) $\chi^{\mathrm{NR}}_{\mathrm{S_0}} = 0$

$$\text{(Raman term) } \chi^{\mathrm{R}}_{\mathrm{S_0}} = C_{\mathrm{S_0}} \sum_i \frac{A_i}{\Omega_i - (\omega_1 - \omega_2) + \mathrm{i}\Gamma_i}$$

$C_{\mathrm{S_0}}$: concentration of S_0 DPA

Susceptibility of Transient Species of DPA

$$\chi_{\mathrm{TR}} = \chi^{\mathrm{el}}_{\mathrm{TR}} + \chi^{\mathrm{R}}_{\mathrm{TR}}$$

$$\text{(electronic term) } \chi^{\mathrm{el}}_{\mathrm{TR}} = C_{\mathrm{TR}} A^{\mathrm{el}} \exp(\mathrm{i}\theta^{\mathrm{el}})$$

$$\text{(Raman term) } \chi^{\mathrm{R}}_{\mathrm{TR}} = C_{\mathrm{TR}} \sum_i \frac{A_i \exp(\mathrm{i}\theta_i)}{\Omega_i - (\omega_1 - \omega_2) + \mathrm{i}\Gamma_i}$$

C_{TR}: concentration of transient species of DPA
Ω_i: Raman frequency

calculated spectra is good. The obtained parameters of the S_1 DPA are summarized in Table 2, and those of the S_2 DPA in Table 3. It is noted that the values of the bandwidths (Γ's) and angles (θ's) are similar for normal-DPA and ^{13}C-DPA except for the two bands of the S_1 DPA at ∼1560 cm^{-1}. Spectral shapes of these two bands are drastically changed in their positions and intensities upon the ^{13}C-substitution. This suggests that the normal modes of these bands are also largely changed. Therefore it is reasonable that the Γ's and θ's of these bands are different for normal-DPA and ^{13}C-DPA. The parameters of the S_2 band around 1130 cm^{-1} seem to be less accurate than those of other bands, because there the S_1 band is overlapping in the same region. The S_2 and S_1 bands are also overlapping around 970 cm^{-1}. Nevertheless the parameters of the 976 cm^{-1} band of the S_2 DPA are expected to be as accurate as those of other bands, because the intensity of this band is much larger than those of the two S_1 bands in this spectral region.

TABLE 2: Parameters for Raman Susceptibility of S_1 Diphenylacetylene

normal-DPA			^{13}C-DPA			
Ω (cm^{-1})	Γ (cm^{-1})	θ (deg)	Ω (cm^{-1})	Γ (cm^{-1})	θ (deg)	^{13}C shift (cm^{-1})
1577	6	346	1573	6	339	−4
1557	6	51	1535	8	17	−22
1169	7	305	1170	7	319	+1
1126	7	344	1122	6	341	−4
987	6	333	987	6	346	0
971	14	295	969	15	272	−2

TABLE 3: Parameters for Raman Susceptibility of S_2 Diphenylacetylene

normal-DPA			^{13}C-DPA			
Ω (cm^{-1})	Γ (cm^{-1})	θ (deg)	Ω (cm^{-1})	Γ (cm^{-1})	θ (deg)	^{13}C shift (cm^{-1})
2099	39	273	2060	40	270	−39
1645	3	215	1645	4	229	0
1194	11	185	1191	12	189	−3
1186	18	313	1186	19	319	0
1127	9	290	1133	7	320	+6
976	6	137	975	6	133	−1
685	19	143	684	18	138	−1

Temporal behavior of the S_1 population was determined by simulating each time-resolved spectrum of the wavenumber region 1700−1400 cm^{-1}. The spectral parameters were fixed to the values in Table 2, and only the concentrations were optimized. The S_1 population obtained by this procedure is plotted against the delay time in Figure 7. The decay curves of the S_1 population are apparently nonexponential. The deviation of the decay curves from single-exponential functions is ascribable to the rotational diffusion of the transient species. Note that the rotational diffusion time for electronically excited 4-(dimethylamino)-4′-cyanodiphenylacetylene is known to be ∼100 ps in cyclohexane at room temperature.[15] For eliminating this effect, the observed points after 200 ps were fitted to exponential functions. The lifetimes thus obtained are 190 ps for normal-DPA and 200 ps for ^{13}C-DPA. These lifetimes are in accordance with the value obtained by time-resolved absorption spectroscopy.[4] The obtained lifetimes may not be so accurate because there seems to remain a small influence of the rotational diffusion even after 200 ps. By fitting the points after 250 ps, we obtained slightly longer lifetimes (210 ps for normal-DPA and 220 ps for ^{13}C-DPA). The accuracy of the

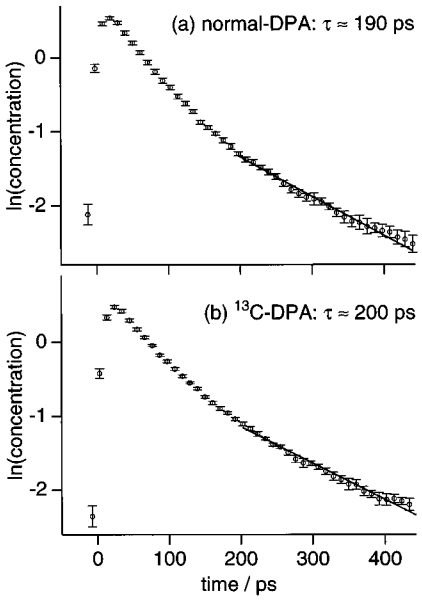

Figure 7. Temporal change of the population of S_1 DPA. (a) normal-DPA, (b) ^{13}C-DPA. Solid lines are fitted curves to single-exponential functions ($e^{-t/\tau}$).

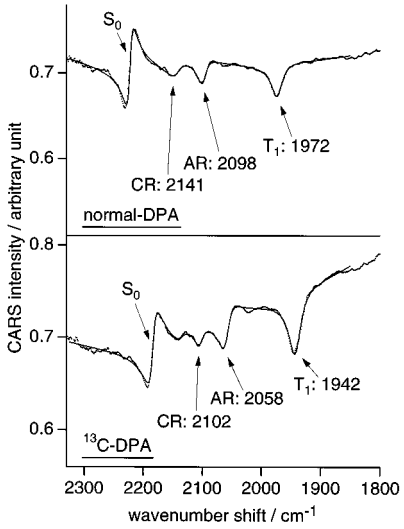

Figure 8. CARS spectral simulation of the C≡C stretch band of the cation radical (CR), the anion radical (AR), and the T_1 state of DPA. Dots show observed data obtained 100−400 ps after the photoexcitation, solid lines simulated spectra.

obtained lifetimes may be estimated to be a few tens of picoseconds. This is good enough to identify this transient species as the S_1 state.

Spectral simulations have been carried out for the C≡C stretch band of the cation radical, the anion radical, and the T_1 state of DPA in a similar manner as in the case of the singlet excited states. We simulated the spectra obtained 100−400 ps after the photoexcitation. No electronic terms for the cation radical, the anion radical, and the T_1 state were included. The results of simulations are shown in Figure 8, and the obtained band parameters are summarized in Table 4. The agreement of the simulated spectra with the observed spectra is good. It is noted that the spectral feature due to the interference between the S_0 band and the cation band in the ^{13}C-DPA spectrum is successfully reproduced by the simulation. The correlation of the obtained bandwidths (Γ's) and angles (θ's) between normal-DPA and ^{13}C-DPA is reasonable, but not as good as in the case of the singlet excited states. This is probably due to the weak signal of the radical species. The obtained vibrational frequencies of the three transient species agree with those obtained by spontaneous Raman measurements[8] within 7 cm^{-1}.

TABLE 4: Parameters for Raman Susceptibilities of C≡C Stretch Bands of Cation Radical (CR), Anion Radical (AR), and T_1 State of Diphenylacetylene

	CARS			spontaneous Raman[a]	
	Ω (cm^{-1})	Γ (cm^{-1})	θ (deg)	Ω (cm^{-1})	assignment
normal-DPA	2141	16	20	2142	C≡C str of CR
	2098	9	54	2091	C≡C str of AR
	1972	12	77	1974	C≡C str of T_1
^{13}C-DPA	2102	11	37	2103	C≡C str of CR
	2058	11	31	2053	C≡C str of AR
	1942	13	76	1942	C≡C str of T_1

[a] From ref 8.

Vibrational Assignments and the Structure of the Excited Singlet States. Drastic changes are observed in the 2100−2000 cm^{-1} region of the S_2 spectrum and in the 1600−1500 cm^{-1} region of the S_1 spectrum upon ^{13}C-substitution. It is clear that the bands in these regions contain large contributions from the central CC stretch vibration. On the other hand, the spectra of the S_2 and S_1 states in other wavenumber regions do not show large frequency shifts and do not change in their intensity patterns upon ^{13}C-substitution. The small change in the intensity pattern indicates that the vibrational modes in these regions do not change much upon ^{13}C-substitution. In the following, we first discuss briefly the vibrational assignments of the bands that are not much affected by the ^{13}C-substitution and then go into the detailed analysis of the band containing large contributions of the central CC stretch vibration.

The 1194 cm^{-1} band of S_2 DPA shows a 3 cm^{-1} downshift and the 1126 cm^{-1} band of S_1 DPA shows a 4 cm^{-1} downshift upon ^{13}C-substitution. Although these shifts are small, they indicate that these bands contain some contributions from the C-phenyl stretch mode. Such small downshifts upon ^{13}C-substitution are also reported for the C-phenyl stretch of the S_0 state (1 cm^{-1}) and the cation radical (4 cm^{-1}) of DPA.[8] The 1186, 1127, 976, and 685 cm^{-1} bands of the S_2 DPA and the 1169, 987, and 971 cm^{-1} bands of the S_1 DPA may be assigned to the vibrational modes of the phenyl rings.[16] For accurate and detailed assignments of these bands, it is necessary to measure the CARS spectra of isotopic analogues of DPA in which the atoms of the phenyl rings are substituted by isotopes.

There is one band at 1645 cm^{-1} in the S_2 CARS spectrum. This band does not show frequency shift upon ^{13}C-substitution. No bands of the S_2 state are observed in the 1600−1500 cm^{-1} region. We therefore assign this band to the phenyl ring CC stretch (probably 8a-like) mode. The frequency 1645 cm^{-1} of S_2 DPA is higher than that of the corresponding band of the S_0 DPA (1596 cm^{-1}).[8] This suggests that the CC bond order in the phenyl groups is larger in the S_2 state than in the S_0. This increase in the CC bond order contrasts with the cases of the cation radical (1590 cm^{-1}), the anion radical (1582 cm^{-1}), and the T_1 state (1565 cm^{-1}) of DPA,[8] in which the phenyl CC bond order decreases.

We now focus on the central CC vibration that is the most characteristic probe of the structure of DPA. The very broad 2099 cm^{-1} band of the S_2 state shifts down by 39 cm^{-1} upon ^{13}C-substitution. The expected downshift for a pure CC stretch is 41 cm^{-1} ($=2099[1-\sqrt{(1/12+1/13)/(1/12+1/12)}]$), and the

observed downshift is 95% of this value. Therefore, the 2099 cm^{-1} band is assignable to a pure central CC stretch mode. The CC stretch frequency of the S_2 state thus identified is 118 cm^{-1} lower than that (2217 cm^{-1}) of the S_0 state.[8] This large downshift indicates that the central CC bonding is weaker in the S_2 state than in the S_0 state. It should be noted that the CC stretch frequency in the S_2 state is still in the "triple-bond stretch region". This suggests a linear structure of DPA in the S_2 state with a triple-bond character of the central CC bond.

The 1577 and 1557 cm^{-1} bands of the S_1 state of normal-DPA shift to 1573 and 1535 cm^{-1} in ^{13}C-DPA. No strong band was observed in the frequency region 2600−1600 cm^{-1} which is assignable to the S_1 state. We conclude that these two bands are contributed from the central CC stretch vibration. The change of the relative intensity of the two bands upon the ^{13}C-substitution indicates that the CC stretch and other vibrations contribute to these bands and that their relative contributions change with ^{13}C-substitution. To further elucidate this relative intensity change in the S_1 state due to the mode mixing, we use a simple two-coordinate model. In this model, we assume that the vibrational modes of the two CARS bands in the 1600−1500 cm^{-1} region are linear combinations of two internal coordinates (s_1 and s_2), where s_1 is the pure central CC stretch coordinate that includes only the motions of the two central carbon atoms and s_2 is a coordinate (for example the 8a-like mode of the phenyl rings) that is orthogonal to s_1. We carry out a two-dimensional GF calculation[17] based on these coordinates. The diagonal **G** matrix element G_{11} can be calculated using the atomic weights of the central carbons, G_{22} is taken as an unknown parameter, and the off-diagonal **G** matrix elements (G_{12}, G_{21}) are zero:

$$\mathbf{G} = \begin{pmatrix} G_{11} & 0 \\ 0 & G_{22} \end{pmatrix}$$

$$G_{11} = \begin{cases} 1/12 + 1/12: \text{ for normal-DPA} \\ 1/12 + 1/13: \text{ for } ^{13}\text{C-DPA} \end{cases}$$

The **F** matrix is symmetric and has three independent element (F_{11}, F_{22}, F_{12}) which are taken as unknown parameters:

$$\mathbf{F} = \begin{pmatrix} F_{11} & F_{12} \\ F_{12} & F_{22} \end{pmatrix}$$

G and **F** matrices can be diagonalized by an **L** matrix. **L** is defined by the following equations.

$${}^t\mathbf{L}\mathbf{G}^{-1}\mathbf{L} = \begin{pmatrix} 1 & 0 \\ 0 & 1 \end{pmatrix}$$

$${}^t\mathbf{L}\mathbf{F}\mathbf{L} = \begin{pmatrix} \lambda_m & 0 \\ 0 & \lambda_n \end{pmatrix}$$

λ_a ($a = m, n$) is related to the frequency of the ath normal mode $\tilde{\nu}_a$ by

$$\tilde{\nu}_a[\text{cm}^{-1}] = 1302.83\sqrt{\lambda_a\left[\frac{\text{mdyn/Å}}{\text{atomic mass unit}}\right]}$$

λ_α and **L** can be expressed as

$$\lambda_m = (A + B - \alpha)/2$$

$$\lambda_n = (A + B + \alpha)/2$$

$$\mathbf{L} = \begin{pmatrix} L_{1m} & L_{1n} \\ L_{2m} & L_{2n} \end{pmatrix}$$

$$L_{1m} = \frac{\sqrt{G_{11}}(A - B - \alpha)}{\sqrt{(A - B - \alpha)^2 + 4C^2}}$$

$$L_{2m} = \frac{\sqrt{G_{22}}2C}{\sqrt{(A - B - \alpha)^2 + 4C^2}}$$

$$L_{1n} = \frac{\sqrt{G_{11}}(A - B + \alpha)}{\sqrt{(A - B + \alpha)^2 + 4C^2}}$$

$$L_{2n} = \frac{\sqrt{G_{22}}2C}{\sqrt{(A - B + \alpha)^2 + 4C^2}}$$

$$A \equiv F_{11}G_{11}, \quad B \equiv F_{22}G_{22}, \quad C \equiv \sqrt{F_{12}{}^2 G_{11}G_{22}}$$

$$\alpha \equiv \sqrt{(A - B)^2 + 4C^2}$$

It is noted that λ_m and λ_n are functions of A, B, and C. Because G_{11} can be calculated using the atomic weights of the central carbons, F_{11}, $F_{22}G_{22}$, and $\sqrt{F_{12}{}^2 G_{22}}$ are parameters that can be determined from the four observed frequencies of normal-DPA and ^{13}C-DPA. Potential energy distributions (PEDs) can be expressed as

$$(\text{PED})_{1m} \equiv \frac{F_{11}L_{1m}{}^2}{\lambda_m} = \frac{A(A - B - \alpha)^2}{[(A - B - \alpha)^2 + 4C^2]\lambda_m}$$

$$(\text{PED})_{2m} \equiv \frac{F_{22}L_{2m}{}^2}{\lambda_m} = \frac{B4C^2}{[(A - B - \alpha)^2 + 4C^2]\lambda_m}$$

$$(\text{PED})_{1n} \equiv \frac{F_{11}L_{1n}{}^2}{\lambda_n} = \frac{A(A - B + \alpha)^2}{[(A - B + \alpha)^2 + 4C^2]\lambda_n}$$

$$(\text{PED})_{2n} \equiv \frac{F_{22}L_{2n}{}^2}{\lambda_n} = \frac{B4C^2}{[(A - B + \alpha)^2 + 4C^2]\lambda_n}$$

where $(\text{PED})_{ia}$ is the contribution of the s_i coordinate to the ath normal mode. $(\text{PED})_{ia}$ is also a function of A, B, and C; thus it can be determined from the observed frequencies. In Table 5 are shown the calculated frequencies, PED, F_{11}, $F_{22}G_{22}$, and $\sqrt{F_{12}{}^2 G_{22}}$, which are determined by the least-squares method. According to the calculated PED, both the 1577 and 1557 cm^{-1} bands of normal-DPA contain ∼50% contributions from the coordinate s_1 and ∼50% contributions from s_2. The 1573 cm^{-1} band of ^{13}C-DPA is contributed mainly from s_2, and the 1535 cm^{-1} band of ^{13}C-DPA is contributed mainly from s_1. If we assume that the observed intensities of ^{13}C-DPA are the intrinsic intensities of the s_1 and s_2 modes, we can argue that the stronger 1577 cm^{-1} band and the weaker 1557 cm^{-1} band of normal-DPA are generated as a result of the in-phase and out-of-phase mode mixing between s_1 and s_2. In this way, the frequency

TABLE 5: Results of the Two-Coordinate GF Calculation for the Mode Mixing in the 1500 cm^{-1} Region of Normal- and ^{13}C-DPA[a]

	observed frequency (cm^{-1})	calculated frequency (cm^{-1})	PED (%)	
			s_1	s_2
normal-DPA	1577	1578.1	44	54
	1557	1558.1	56	46
^{13}C-DPA	1573	1571.9	7	92
	1535	1533.9	93	8

[a] Determined parameters: $F_{11} = 8.682$ mdyn/Å; $F_{22}G_{22} = 1.451$ mdyn/(Å atomic mass unit); $\sqrt{F_{12}^2 G_{22}} = 0.04500$ mdyn/(Å $\sqrt{\text{atomic mass unit}}$). Square root of diagonal GF product: 1302.83 $\sqrt{F_{11}G_{11}} = 1567.2$ cm^{-1} (normal-DPA), 1536.6 cm^{-1} (^{13}C-DPA); 1302.83 $\sqrt{F_{22}G_{22}} = 1569.2$ cm^{-1}.

shifts and the relative intensity change upon the ^{13}C-substitution are semiquantitatively explained with this simple two-coordinate model.

The intrinsic CC stretch frequency of S_1 DPA deduced from the two-coordinate model is 1567 cm^{-1}, which is in the typical frequency region for a CC double-bond stretch vibration. This fact suggests that the structure of the central part of DPA changes drastically in the S_1 state and the CC bond becomes double-bond-like rather than triple. This conclusion is consistent with the results of the semiempirical CI calculation by Ferrante et al., which includes 200 energy-selected configurations.[7] They calculated the potential energy curves of the four low-lying excited states (1^1B_{1u}, 1^1B_{2u}, 1^1B_{3g}, 1^1A_u) of DPA along the central CC bond length with other geometric parameters fixed to those of S_0 DPA. According to their results, the potential curves of the 1^1B_{1u} state and 1^1A_u state have their minima at different CC bond lengths. The energy minimum of the 1^1A_u potential is lower than that of the 1^1B_{1u} potential, though the 1^1B_{1u} state is the lowest excited singlet state at the CC bond length of the S_0 state. The 1^1A_u state is the "real" S_1 state in the sense that the minimum energy of this state is the lowest among those of the four excited singlet states. The CC bond length at the 1^1A_u potential minimum is calculated to be 1.280 Å, which is closer to a typical double-bond value rather than to that of a triple bond. The very long bond length explains the observed low frequency of the CC stretch mode of S_1 DPA. The CC bond length at the 1^1B_{1u} potential minimum is calculated to be 1.245 Å, which is a little longer than the CC bond length of S_0 DPA (1.200 Å). This bond length is consistent with the observed ~100 cm^{-1} downshift of the CC stretch frequency in the S_2 state. It seems certain that the observed S_2 and S_1 states correspond to the calculated 1^1B_{1u} and 1^1A_u states, respectively. A large decrease of the CC bond order in the S_1 state is well-known for the acetylene molecule[18] that has a trans-bent form with the CC stretch frequency of 1385 cm^{-1}. The symmetry species of the S_1 acetylene is considered to be A_u, as in the case of S_1 DPA. Therefore, it is quite likely that S_1 DPA has also a bent structure (trans- or cis-form) as in the case of acetylene in the S_1 state. To clarify this point, observations of the infrared absorption of S_1 DPA are desirable. A high-level MO calculation with full geometry optimization may also be helpful.

$S_2 \rightarrow S_1$ Internal Conversion Process. We have shown experimentally that the structure of the central CC part of DPA changes markedly on going from S_2 to S_1. The central CC part of DPA has a double-bond-like structure in the S_1 state, and it retains the triple-bond-like structure in the S_2 state. The $S_2 \rightarrow S_1$ internal conversion process must be accompanied by a structural change at the central CC part. Therefore, the internal conversion process can be regarded as a kind of isomerization, as was already pointed out by Ferrante et al.[7] The extremely large bandwidth ($\Gamma \approx 40$ cm^{-1}) of the CC stretch mode in the S_2 state is of great interest in relation to the isomerization dynamics. In the case of S_1 *trans*-stilbene, a linear relationship between the olefinic C═C stretch bandwidth and the trans−cis isomerization rate was found and was discussed in relation to a new vibrational dephasing mechanism.[19,20] A similar relationship may exist between the S_2 CC stretch bandwidth and the $S_2 \rightarrow S_1$ isomerization rate of DPA. Further experiments including temperature dependence will make this point clear.

Acknowledgment. The experimental part of this work was carried out at Kanagawa Academy of Science and Technology.

References and Notes

(1) Tanizaki, Y.; Inoue, H.; Hoshi, T.; Shiraishi, J. *Z. Phys. Chem.* **1971**, NF *74*, 45.
(2) Okuyama, K.; Hasegawa, T.; Ito, M.; Mikami, N. *J. Phys. Chem.* **1984**, *88*, 1711.
(3) Gutmann, M.; Gudipati, M.; Schönzart, P.-F.; Hohlneicher, G. *J. Phys. Chem.* **1992**, *96*, 2433.
(4) Hirata, Y.; Okada, T.; Mataga, N.; Nomoto, T. *J. Phys. Chem.* **1992**, *96*, 6559.
(5) Hirata, Y.; Okada, T.; Nomoto, T. *Chem. Phys. Lett.* **1993**, *209*, 397.
(6) Hirata, Y.; Okada, T.; Nomoto, T. *J. Phys. Chem.* **1993**, *97*, 9677.
(7) Ferrante, C.; Kensy, U.; Dick, B. *J. Phys. Chem.* **1993**, *97*, 13457.
(8) Hiura, H.; Takahashi, H. *J. Phys. Chem.* **1992**, *96*, 8909.
(9) Ishibashi, T.; Hamaguchi, H. *Chem. Phys. Lett.* **1994**, *264*, 551.
(10) Tahara, T.; Hamaguchi, H. *Rev. Sci. Instrum.* **1994**, *65*, 3332. Tahara, T.; Toleutaev, B. N.; Hamaguchi, H. *J. Chem. Phys.* **1994**, *100*, 786.
(11) Stephens, R. D.; Castro, C. E. *J. Org. Chem.* **1963**, *28*, 3313.
(12) Castro, C. E.; Gaughan, E. J.; Owsley, D. C. *J. Org. Chem.* **1966**, *31*, 4071.
(13) Toleutaev, B. N.; Tahara, T.; Hamaguchi, H. *Appl. Phys. B* **1994**, *59*, 369.
(14) Kinoshita, K.; Hirai, N.; Tsuchiya, Y. *SPIE* **1983**, *348*, 222.
(15) Hirata, Y.; Kanemoto, Y.; Okada, T.; Nomoto, T. *J. Mol. Liq.* **1995**, *65/66*, 421.
(16) The 1127 cm^{-1} band of S_2 DPA apparently shifts 6 cm^{-1} to higher frequency upon ^{13}C-substitution. There remains some uncertainties in the determined frequency of this S_2 band due to the overlapping of the S_1 band. We do not go into the details of this upshift of the 1127 cm^{-1} band.
(17) Wilson, E. B., Jr.; Decius, J. C.; Cross, P. C. *Molecular Vibrations*; McGraw-Hill: New York, 1955.
(18) Ingold, C. K.; King, G. W. *J. Chem. Soc.* **1953**, 2725.
(19) Hamaguchi, H.; Iwata, K. *Chem. Phys. Lett.* **1993**, *208*, 465.
(20) Hamaguchi, H. *Mol. Phys.* **1996**, *89*, 463.